Published in final edited form as:

Eur Biophys J. 2023 July ; 52(4-5): 427–438. doi:10.1007/s00249-023-01648-x.

Strong non-ideality effects at low protein concentrations: considerations for elongated proteins

Alexander E. Yarawsky[1,*,&], **Vlad Dinu**[2], **Stephen E. Harding**[2], **Andrew B. Herr**[1,3,4]

[1]Division of Immunobiology, Cincinnati Children's Hospital Medical Center, Cincinnati, OH, USA

[2]National Centre for Macromolecular Hydrodynamics (NCMH), University of Nottingham, Sutton Bonington, Loughborough, LE12 5RD UK

[3]Division of Infectious Diseases, Cincinnati Children's Hospital Medical Center, Cincinnati, OH, USA

[4]Department of Pediatrics, University of Cincinnati College of Medicine, Cincinnati, OH, USA

Abstract

A recent investigation was aimed at obtaining structural information on a highly extended protein via SEC-MALS-SAXS. Significantly broadened elution peaks were observed, reminiscent of a phenomenon known as viscous fingering. This phenomenon is usually observed above 50 mg/mL for proteins like bovine serum albumin (BSA). Interestingly, the highly extended protein (Brpt5.5) showed viscous fingering at concentrations lower than 5 mg/mL. The current study explores this and other non-ideal behavior, emphasizing the presence of these effects at relatively lower concentrations for extended proteins. BSA, Brpt5.5, and a truncated form of Brpt5.5 referred to as Brpt1.5 are studied systematically using size-exclusion chromatography (SEC), sedimentation velocity analytical ultracentrifugation (AUC), and viscosity. The viscous fingering effect is quantified using two approaches and is found to correlate well with the intrinsic viscosity of the proteins – Brpt5.5 exhibits the most severe effect and is the most extended protein tested in the study. By AUC, the hydrodynamic non-ideality was measured for each protein via global analysis of a concentration series. Compared to BSA, both Brpt1.5 and Brpt5.5 showed significant non-ideality that could be easily visualized at concentrations at or below 5 mg/mL and 1 mg/mL, respectively. A variety of relationships were examined for their ability to differentiate the proteins by shape using information from AUC and/or viscosity. Furthermore, these relationships were also tested in the context of hydrodynamic modeling. The importance of considering non-ideality when investigating the structure of extended macromolecules is discussed.

[&]Corresponding author: ayarawsky@bioanalysisllc.com.
[*]Current address: BioAnalysis, LLC, 3401 I Street Suite 206 Philadelphia, PA 19134, USA

Author contributions

A.E.Y. conceived the project, designed experiments, performed experiments, analyzed data, and wrote the manuscript
V.D. designed experiments, performed experiments, and analyzed data
S.E.H. guided analysis and reviewed the manuscript
A.B.H. designed experiments and provided funding
All authors reviewed the manuscript and contributed significantly to the final product.

Competing Interests: A.B.H. serves as a Scientific Advisory Board member for Hoth Therapeutics, Inc., holds equity in Hoth Therapeutics and Chelexa BioSciences, LLC, and was a co-inventor on seven patents broadly related to proteins described in this study.

Keywords

Hydrodynamic non-ideality; viscosity; sedimentation velocity; global analysis; hydrodynamic modeling; viscous fingering

Introduction

There is a long history of interest in the structure of proteins. High-resolution techniques such as X-ray crystallography, NMR, and more recently cryo-EM, are common practice among protein structure labs. Many proteins, however, are not amenable to crystallization, while NMR and cryo-EM require very expensive instrumentation. Additionally, crystallography and cryo-EM approaches require removal of the protein from its native solution environment. Biologically relevant protein assembly can also be difficult to distinguish from crystal packing (Elez et al. 2018; Luo et al. 2015).

Hydrodynamic approaches have a long track record of offering a vast array of complementary biophysical and mechanistic information, including shape, molar mass, homogeneity, stability, and aggregation propensity. Analytical ultracentrifugation (AUC) was developed in the 1920's by Theodore Svedberg, when he performed sedimentation equilibrium experiments to determine the molecular weight of ovalbumin, hemoglobin, phycocyanin, and phycoerythrin in various buffers (Svedberg and Fåhraeus 1926; Svedberg and Lewis 1928; Svedberg and Nichols 1926; Svedberg and Nichols 1927). There also exists a rich history in the use of viscosity to determine macromolecular shape and flexibility parameters, dating back to Einstein in the early 1900's (Einstein 1906; Einstein 1911; Harding 1995; Harding 1997).

During a previous structural investigation of a fibril-like protein, very broad and abnormally shaped SEC elution peaks were observed, despite a highly pure and homogeneous sample (Yarawsky et al. 2022). The elution behavior was reminiscent of a phenomenon known as viscous fingering, which is often observed at high concentrations (~50 mg/mL) for proteins like bovine serum albumin (BSA) (Plante et al. 1994). This phenomenon can also be observed when the injected sample is spiked with dextran to increase the viscosity of the sample (Flodin 1961). The root cause of the effect is the fingering that occurs at the interface between a more viscous solution and a less viscous solvent.

To better understand why this protein showed such prominent viscous fingering while at relatively low concentrations (Yarawsky et al. 2022), a systematic analysis of several proteins was performed. The protein construct with which the observations were made previously – Brpt5.5 – is part of the B-repeat superdomain of the biofilm-related accumulation-associated protein (Aap) from *Staphylococcus epidermidis*. The Brpt5.5 construct contains 5 full B-repeats and a C-terminal half-repeat. For comparative purposes, an additional construct containing one and a half B-repeats (Brpt1.5) is also examined here. The Brpt1.5 construct has been extensively studied to show that it exists in solution as an extended monomer (Chaton and Herr 2017; Conrady et al. 2008; Conrady et al. 2013; Shelton et al. 2017). The Brpt5.5 construct has been characterized by extensive hydrodynamic analyses and small-angle X-ray scattering (SAXS), which demonstrated that

Brpt5.5 is monomeric and lacked any significant flexibility (Yarawsky and Herr 2020; Yarawsky et al. 2022; Yarawsky et al. 2020). It is worth noting that the biological function of the B-repeat superdomain is to assemble in the presence of Zn^{2+} into amyloid-like fibrils that contribute toward the strength and stability of *S. epidermidis* biofilms. This self-association often requires millimolar concentrations of Zn^{2+} in the context of purified protein in solution and does not assemble as an apo-protein (Chaton and Herr 2017; Shelton et al. 2017; Yarawsky and Herr 2020). In the current study, Brpt1.5 and Brpt5.5 were only studied in the monomeric form. In addition, bovine serum albumin (BSA) was examined as a protein with a globular conformation. This is in stark contrast to the Brpt1.5 and Brpt5.5 proteins, as seen in Figure 1.

This study investigates the impact of shape on hydrodynamic behavior, especially as it relates to size-exclusion chromatography, sedimentation velocity AUC, and viscosity. It demonstrates the clear ability of hydrodynamic techniques to provide structural insights. Additionally, the importance of considering and measuring non-ideality in sedimentation velocity experiments is discussed. Oftentimes, proteins are assumed to behave ideally in “dilute” solutions. However, it is difficult to know at what point it is reasonable to assume that non-ideality is not impacting the data without having collected data at multiple concentrations. Brpt5.5 provides an excellent example of a protein that behaves non-ideally at concentrations below 1 mg/mL – where many investigators may assume an ideal species.

Results

Viscous fingering at low concentrations

Each protein was purified and dialyzed into matching 20 mM Tris, 150 mM NaCl (pH 7.4) buffer. Next, the proteins were analyzed by SEC using a Superose 6 (24 mL) column with an injection volume of 250 μL and flow rate of 0.5 mL/min at 4°C. Figure 2 shows the elution profile for (A) BSA, (B) Brpt1.5, and (C) Brpt5.5. While BSA required a 25 mg/mL loading concentration before significant peak broadening occurred, Brpt1.5 and Brpt5.5 showed a similar effect at 10 mg/mL and 4 mg/mL loading concentrations, respectively. To better quantify the severity of the viscous fingering, the height equivalent of a theoretical plate (HETP) and asymmetry factor (A_s) were calculated for each elution (Figure 2D and Figure 2E). These are parameters commonly used to evaluate column performance. Higher values indicate peak broadening and tailing associated with poor column performance. However, the HETP parameter has also been used to quantify viscous fingering effects (Plante et al. 1994). From the results shown in Figure 2, it is very apparent that Brpt5.5 displays viscous fingering effects at much lower concentrations than BSA.

Intrinsic viscosity correlates with shape

Given that the viscosity of the injected solution is relevant to the severity of viscous fingering, it could be inferred that a solution of Brpt5.5 would have a higher viscosity than a solution of BSA at the same protein concentration. The viscosity of protein solutions may also be directly measured using a capillary viscometer. Figure 3A shows the measured relative viscosity (η_{rel}) of solutions of BSA, Brpt1.5, and Brpt5.5. A trend was observed

that reflected the HETP results very closely, confirming that the viscous fingering effects observed by SEC were in fact due to increased viscosity of Brpt1.5 and Brpt5.5.

The reduced specific viscosity (η_{red}), inherent viscosity ((ln η_{rel})/c), and intrinsic viscosity ([η]) were determined at multiple concentrations, as plotted in Figure 3 for each protein. Extrapolation to zero concentration removes concentration-dependent effects and provides the fundamental macromolecular information. The intrinsic viscosity is particularly useful in its relationship to macromolecular conformation, flexibility, and hydration. Macromolecules that exhibit high axial ratios also show high intrinsic viscosities (Creeth and Knight 1965; Harding 1997). The intrinsic viscosities measured for Brpt1.5 and Brpt5.5 are indeed much greater than BSA, correlating well with the more extended shapes of Brpt1.5 and Brpt5.5.

Hydrodynamic non-ideality measured by sedimentation velocity AUC

High intrinsic viscosity is correlated with an increase in the hydrodynamic non-ideality term, k_s, for extended macromolecules (Creeth and Knight 1965; Harding 1997). The hydrodynamic non-ideality term is related to the backflow of solvent displaced by the macromolecule as it sediments through solution in a closed system, and it is a concentration-dependent phenomenon (Correia and Stafford 2015). Sedimentation velocity experiments were performed across a concentration range to determine the hydrodynamic non-ideality of each protein.

Figure 4 shows g(s*) distributions and WDA (wide distribution analysis) distributions obtained from sedimentation velocity experiments. The g(s*) analysis requires a short time span of data to be used, while the WDA uses all scans collected during the experiment. Both are based on the time-derivative of the concentration profile and are considered model-independent analyses of the data (Philo 2000; Sherwood and Stafford 2016; Stafford 1992). For a case such as this, where non-ideality is of interest, a model-independent approach is preferred over the c(s) analysis that assumes ideal, noninteracting species (Schuck 2000). In both the g(s*) and WDA distribution, the effect of hydrodynamic non-ideality is visually apparent. In accordance with Equation 1 and Equation 2, an increase in the $k_s c$ term results in a slowing and sharpening of the sedimentation boundary (Correia et al. 2020).

$$s(c) = \frac{s^0}{(1 + k_s c)} \quad \text{(Equation 1)}$$

$$D(c) = \frac{D^0(1 + 2BM_1 c)}{(1 + k_s c)} \quad \text{(Equation 2)}$$

Once again, the concentration of Brpt1.5 and Brpt5.5 required to observe a similar effect to BSA is much lower. For example, a significant shift in the g(s*) distribution is observed for BSA at 3 – 8.7 mg/mL, while just 0.68 mg/mL of Brpt5.5 showed a significant shift.

Two basic approaches exist to quantify the k_s value. The first approach directly fits the relationship between the sedimentation coefficient ($s_{20,w}$) and the loading concentration (Correia et al. 2016; Correia et al. 2020; Winzor et al. 2021). The $1/s_{20,w}$ vs concentration

plots are shown in Figure 5, along with a standardized plot ($s_{20,w}/s^0_{20,w}$) to show the relative impact of hydrodynamic non-ideality on the sedimentation coefficient. The extreme effect of hydrodynamic non-ideality on the sedimentation of Brpt5.5 is easily visualized in Figure 5D, where at 1 mg/mL, BSA, Brpt1.5, and Brpt5.5 show decreasing values of 0.985, 0.975, and 0.923, respectively.

A more rigorous approach is to globally fit the data using direct boundary fitting in SEDANAL (Correia et al. 2020; Sherwood and Stafford 2016). Because sedimentation and diffusion both impact the sedimentation boundaries, a model containing both the hydrodynamic non-ideality (k_s) and thermodynamic non-ideality (BM_1) terms should be fitted. The thermodynamic non-ideality term is expected to be on the same order of magnitude as k_s but is less well-determined by velocity experiments – especially when experiments are run at a high speed to minimize the impact of diffusion with respect to sedimentation. The results of SEDANAL fitting to a non-ideal model are listed in Table 1 and are comparable to the result from linear fitting of the $s_{20,w}$ vs concentration data. Figure S1 – Figure S3 shows the quality of fit for each global analysis. Characterization of the concentration-dependence of the sedimentation coefficient also yields the $s^0_{20,w}$ value. The k_s values are again increasing with protein shape (BSA < Brpt1.5 < Brpt5.5). The especially high k_s value of Brpt5.5 helps explain why the g(s*) distribution shows significant slowing and sharpening even below 1 mg/mL (Figure 4).

Determination of shape from AUC

A parameter of interest for biophysicists and structural biologists alike is the shape of the macromolecule. In the absence of high-resolution structural data, sedimentation velocity AUC experiments can provide very reliable indications of the macromolecule's global conformation in solution. The Svedberg Equation and Stokes-Einstein Equation relate the sedimentation coefficient (s), the diffusion coefficient (D), the buoyant mass (M_b), and the frictional coefficient (f) (Chaton and Herr 2015; Correia and Stafford 2015; Rocco and Byron 2015b). Rather than reporting the frictional coefficient, the more useful parameter is the frictional ratio (f/f_0). This is the ratio of the frictional coefficient of the solute to the frictional coefficient of an ideal sphere of the same volume and offers a shape description that is independent of the macromolecule's size. Accurate determination of the f/f_0 relies on accurate fitting of the concentration-dependence of s and D. Where non-ideality is present, this means also fitting both the hydrodynamic and thermodynamic non-ideality terms.

A common approach to determining f/f_0 is to utilize the c(s) analysis implemented in SEDFIT. However, considering the major concentration-dependence of both s and D due to non-ideality, global fitting to a non-ideal model is required. For illustrative purposes, Table S1 lists the s, M, and f/f_0 for each individual dataset analyzed by c(s). The higher concentration datasets could be interpreted as highly extended dimer or trimers. A similar discrepancy is observed when fitting g(s*) distributions in DCDT+. This is simply due to the impact of k_sc (and BM_1c) on s and D. It should be noted that the quality of these fits to ideal models is quite poor, so careful analysis by the user should avoid such erroneous results from being reported.

Direct boundary fitting performed in SEDANAL to the non-ideal model used previously was therefore used to determine the f/f_0 (at infinite dilution). An alternative approach would be to use the fitted $s^0_{20,w}$ and M to calculate f/f_0. The SEDANAL-fitted f/f_0 was incorporated into Table 2 with error estimates for each protein. Using X-ray crystallography structures of BSA and Brpt1.5, and a SAXS-validated structure of Brpt5.5, a comparison of the experimentally determined f/f_0 and theoretical f/f_0 from hydrodynamic modeling could be compared. Good agreement with hydrodynamic modeling via HullRadSAS (Fleming et al. 2023; Fleming and Fleming 2018) (Table 3) indicates that AUC can be effectively used to estimate the shape of highly non-ideal macromolecules.

Evaluation of shape parameters using viscosity and AUC data

Many studies have been performed utilizing *either* hydrodynamic data from AUC *or* viscosity data have been utilized to gain structural insights into macromolecules. Because both sets of data have been collected and structures have already been determined for the proteins of interest, the current study provides an excellent opportunity to evaluate various relationships often used in the field. Creeth and Knight published a seminal review focused on estimation of shape from sedimentation and viscosity data (Creeth and Knight 1965). Since then, additional work has been focused on further developing these approaches and has been summarized by Harding (Harding 1995).

The ratio of intrinsic viscosity ([η]) over partial specific volume ($\bar{v}$ or "v-bar") known as the viscosity increment (ν) is expected to yield a ratio of 2.5 for spheres but increases with asymmetry. The f/f_0 has already been discussed above, where a value of 1.0 would indicate an anhydrous, ideal hard sphere. Globular proteins often are expected to exhibit a f/f_0 ~1.2–1.3. More specific shape information can be obtained from the Perrin function (P). This parameter distinguishes between contributions of molecular shape and hydration (requiring hydration information), and it can be used to define the axial ratio (a/b) of a prolate or oblate ellipsoid (Harding 1995) using the ELLIPS1 software (Harding et al. 1997). Equations describing both the viscosity increment and f/f_0 can be used to produce the Scheraga-Mandelkern β function. The result is independent of hydration, but requires very accurate experimental determination of s, [η], M, and $\bar{v}$, and is often considered to be rather insensitive to shape (Creeth and Knight 1965; Harding 1995).

Analyses of k_s and [η] by Wales and van Holde indicate that k_s/[η] provides a shape parameter that is sensitive to global conformation and does not require any assumptions about hydration. A ratio of ~1.6 is expected for globular proteins, while asymmetry pushes the ratio lower. The Wales-van Holde ratio is a highly attractive parameter to describe shape, given that both k_s and [η] can be readily measured.

With high-resolution structures or SAXS-based models available for the three proteins, it is possible to perform hydrodynamic bead modeling (Bujacz 2012; Conrady et al. 2013; Yarawsky et al. 2022). This allows for comparison of predicted vs experimental $s^0_{20,w}$, f/f_0, a/b, intrinsic viscosity, and k_s values from HullRadSAS (Fleming et al. 2023; Fleming and Fleming 2018). An additional approach was taken using the AtoB bead modeling approach with ZENO hydrodynamic calculations, as implemented in US-SOMO (Brookes et al. 2010; Byron 1997; Juba et al. 2017; Kang et al. 2004; Rocco and Byron 2015a). Overall, the

hydrodynamic predictions are in reasonable agreement with the experimental parameters. The major discrepancy is in the a/b ratio derived from the Perrin (P) function, which severely overestimated the degree of extension in the molecules in reference to the estimate by the Scheraga-Mandelkern β function and hydrodynamic modeling. Hydrodynamic predictions tend to be especially useful when evaluating the plausibility of several different conformational models, rather than describing the exact shape and dimensions of a given molecule in solution (Brautigam et al. 2020; Marx et al. 2020; Monsen et al. 2021; Rocco and Byron 2015b; Yarawsky et al. 2022). Despite minor inconsistencies in the hydrodynamic predictions and experimental data, it is very clear that there is increasing extension from BSA to Brpt1.5 and Brpt5.5.

Discussion

The goal of this study was to examine the interplay between viscous fingering in chromatography and non-ideal sedimentation. Viscosity measurements demonstrated that the aberrant elution profiles observed, especially for Brpt5.5 at concentrations below 5 mg/mL, were indeed due to high solution viscosity. The increased viscosity of Brpt5.5 also correlated with strong hydrodynamic non-ideality measured by sedimentation velocity AUC, which presents itself via a slowing and sharpening of the g(s*) distribution. An advantage of including Brpt1.5 in this study was to demonstrate the effect of increased axial ratio, without significantly changing the secondary structure or amino acid composition of the protein. Similar comparisons have been performed with fractionated collagen (Nishihara and Doty 1958), however, the present study is able to ensure homogeneity in the samples. In agreement with the collagen data, the longer molecules exhibited higher intrinsic viscosity and hydrodynamic non-ideality (Creeth and Knight 1965). BSA acted as a globular reference and showed results more consistent with a spherical particle. Indeed, the direct ratio of $k_s/[\eta]$ provided a simple indication of extended shape in Brpt1.5 and Brpt5.5, compared to BSA.

The phenomenon of viscous fingering has been traditionally observed in SEC experiments, where a highly viscous sample interfaces with a less viscous solvent. In contrast, sedimentation velocity experiments start with an equal distribution of the sample throughout the AUC cell. Therefore, there is no point at which the solute must interface with a dramatically different solution viscosity – other than at the outer radius of the cell where sedimented solute builds up to high concentrations significant causing back-diffusion. Interestingly, at least one example of fingering in SV-AUC has been reported. This case involved a mixture of albumin and dextran at high concentrations. During the experiment, dextran forms a concentration gradient, thereby forming a density and viscosity gradient across the cell through which albumin must sediment. At the point in time where albumin crosses the dextran gradient, the schlieren profile shows a split peak. This phenomenon was concentration-dependent and could be explained by cross-term diffusion effects (Comper and Preston 1992). Such ternary systems (solvent + 2 solutes) can now be analyzed quantitatively using SEDANAL, which can model the cross-term non-ideality present in the sedimentation and diffusion coefficients (Correia et al. 2016; Stafford 2016).

Beyond sedimentation velocity experiments, approaches such as analytical band centrifugation (Khasa et al. 2021; Schneider and Cölfen 2018; Schneider et al. 2018; Vinograd et al. 1963) and synthetic boundary experiments (Wright et al. 2018) have been shown recent interest within the AUC community. Analytical band centrifugation experiments involve layering a small amount of solute onto the solvent column at the start of acceleration phase in the AUC. The solute then must interface the solvent. Ideally, the solvent will be of slightly higher density than the sample, allowing for a sharper band (Schneider et al. 2018). If a high enough solute concentration exists in the sample to be overlaid, it is expected that viscous fingering could be observed. On the other hand, synthetic boundary experiments do not involve the solute being forced through the solvent via centrifugation (like with SV-AUC) or flow (like with SEC). Instead, solvent is layered on top of a solute-containing column during acceleration, then the solute is allowed to diffuse into the solvent layer. One would not expect that viscous fingering would be observed in synthetic boundary experiments.

Not only does this study demonstrate the effects of shape on non-ideality and viscosity, but it also provides an opportunity to evaluate the usefulness of certain shape parameters and relationships that have been previously proposed and used within the field. A common result presented with sedimentation velocity data is the f/f_0. A value of ~1.3 is expected for globular proteins, while higher values are expected with higher asymmetry. A more explicit shape parameter for ellipsoids is the a/b (axial) ratio. Table 2 lists the a/b ratio derived from the Perrin function and the Scheraga-Mandelkern β function. In comparison with hydrodynamic modeling based on the protein structures, the a/b ratio from the hydration-independent β function is in better agreement than that derived from the Perrin function. Though the β function itself has been considered relatively insensitive to shape changes (for example, 2.45×10^6 vs 2.53×10^6 for Brpt1.5 and Brpt5.5) the a/b ratio derived can still prove to be quite useful. Nevertheless, both derivations of the a/b ratio indicate much greater extension in the Brpt1.5 and Brpt5.5 proteins than in BSA.

While hydrodynamic approaches are unable to provide high-resolution structural information like X-ray crystallography or cryo-EM, they do provide relatively easy access to lower-resolution information. In many cases, it may be sufficient to simply exclude given conformations or models for a protein of interest. To demonstrate this concept, hydrodynamic modeling was performed using HullRadSAS and AtoB/ZENO. Both approaches yielded a/b ratios similar to those derived from the β function and f/f_0 values similar to those experimentally determined. Nonetheless, it is evident how hydrodynamic modeling may be able to provide sufficient information to exclude certain structural models. With the recent advent of new computational approaches for structure prediction such as AlphaFold (Jumper et al. 2021) or Rosetta (Du et al. 2021), it may become more important than ever to understand the capabilities of hydrodynamic approaches like AUC and viscosity measurements, as these provide a relatively simple and effective platform to validate predicted structures.

Materials and Methods

Protein Purification

Bovine serum albumin Fraction V (BP1605–100) was resuspended in 20 mM Tris pH 7.4, 150 mM NaCl and purified via Superdex 200 16/600 pg (Cytiva) to yield pure monomeric BSA. Brpt1.5 was composed of amino acids 2017–2223 from Aap (accumulation-associated protein) from *S. epidermidis* strain RP62A. The protein was expressed as a fusion with a His-MBP tag, which was cleaved via TEV protease as previously described (Conrady et al. 2008). Brpt1.5 was additionally purified by anion exchange using a HiTrap ANX FF 5 mL column (Cytiva). The running buffer was 20 mM Tris pH 7.4, 50 mM NaCl, and an elution gradient was produced using 20 mM Tris pH 7.4, 1 M NaCl. Brpt5.5 was composed of amino acids 1505–2223 from Aap from RP62A and contained an N-terminal His-MBP tag and a C-terminal Strep-II tag. A TEV protease cleavage site was present downstream of the N-terminal tags and upstream of the C-terminal tag (Yarawsky et al. 2022; Yarawsky et al. 2020). The purification of Brpt5.5 was performed as previously described (Yarawsky et al. 2022).

Size Exclusion Chromatography

All SEC data presented were collected using a Superose 6 Increase 10/300 24 mL column (Cytiva) connected to an ÄKTA FPLC system (Cytiva) at 4°C. The column was equilibrated in running buffer (20 mM Tris pH 7.4, 150 mM NaCl). The flow rate was set to 0.5 mL/min and a 250 μL sample was injected. Samples were diluted from a concentrated stock that had been dialyzed overnight into running buffer at 4°C. SEC data were exported from UNICORN and the HETP and A_s values determined manually using Excel and GUSSI (Brautigam 2015). The HETP value was calculated according to Equation 3, where L is the column length (300 mm) and N is the number of theoretical plates, calculated according to the Exponentially Modified Gaussian Model shown in Equation 4 (Jeansonne and Foley 1991).

$$HETP = L/N \quad \text{(Equation 3)}$$

$$N = \frac{41.7(t_r/w)^2}{(a/b) + 1.25} \quad \text{(Equation 4)}$$

The calculation of N used was chosen over other methods to best accommodate asymmetric peaks observed in the presence of viscous fingering. The retention time (t_r) was taken as the weight-average time of the peak of the least concentrated sample. The peak width (w) was the width at 10% of the peak height, with a and b being the distance from t_r and the leading (a) or trailing edge (b) of the peak at 10% max height. The ratio of b/a determined the asymmetry (A_s) value. SEC protein standards (BioRad; #1511901) were used to ensure Superose 6 column performance was adequate (Figure S4). A 100 μL aliquot was injected, while all other parameters were kept equivalent to other the experiments.

Analytical Ultracentrifugation

A Beckman Coulter ProteomeLab XL-I was used to collect interference data at multiple concentrations. Meniscus-matching centerpieces (SpinAnalytical) were used. Data was collected at 48,000 rpm on 4 cells per experiment in an 8-hole rotor (An 50Ti). A radial calibration was performed prior to each experiment. Data collection was monitored using SEDVIEW (Hayes and Stafford 2010). Experiments were carried out until there was no further sedimentation occurring by visual evaluation. To ensure the highest scan frequency and best possible data for g(s^*) and SEDANAL fitting, no time delay between scans was used. To ensure scans be collected throughout the entire sedimentation process, the Equilibrium option was chosen rather than the Velocity option within ProteomeLab. A Method schedule of 100 steps of 99 scans, totaling 9900 scans per cell, instead of the standard 999 scans maximum would be collected. The experiment was stopped manually once sufficient data were collected. Analyses were performed in DCDT+ (Philo 2000; Stafford 1992), SEDANAL (Sherwood and Stafford 2016; Stafford and Braswell 2004; Stafford and Sherwood 2004), and SEDFIT (Schuck 2000). Linear fitting of $1/s_{20,w}$ vs concentration to determine k_s and $s^0_{20,w}$ was performed in SEDNTERP v3 (Laue et al. 1992; Philo 2023). SEDNTERP v3 was also used to estimate buffer density and viscosity, as well as the $\bar{v}$, mass, and extinction coefficients for each protein. Within DCDT+, the g(s^*) distributions were converted to $s_{20,w}$, and the concentration (fringes) and weight-average s value from the time of analysis ($\hat{g}(s^*)$) were used for k_s and $s^0_{20,w}$ determination. The resting rotor temperature of the AUC was determined using a NIST-calibrated DS1922L iButton (iButtonLink) following a procedure previously described (Ghirlando et al. 2014). The measured temperature was incorporated into SEDNTERP for more accurate estimates of the buffer and solute parameters. Error analysis of SEDANAL fits was performed using F-Statistics at a 95% confidence level. The following parameters were allowed to fit: loading concentration, s, k_s, BM_1, and the molar mass or frictional ratio.

Viscosity Measurements

A semi-automated U-tube Ostwald capillary viscometer (Schott Geräte, Hofheim, Germany) was used to measure buffer (t_0) and sample solution (t_s) flow times. Aliquots of 2 mL were prepared at multiple concentrations from dilution of a stock solution, and the relative viscosity (η_r) was calculated according to Equation 5:

$$\eta_r = \frac{\eta_s}{\eta_0} = \left(\frac{t_s}{t_0}\right) \times \frac{\rho_s}{\rho_0} \quad \text{(Equation 5)}$$

which includes the buffer (ρ_0) and solution (ρ_s) density and the buffer (η_0) and solution (η_s) viscosity. The buffer and sample solution density values were assumed to be equivalent. All viscosity experiments were performed at 20°C using samples dialyzed into the same buffer (20 mM Tris pH 7.4, 150 mM NaCl).

The reduced viscosity (η_{red}) was determined according to the Huggins Equation (Huggins 1942) by extrapolation to zero concentration (c).

$$\eta_{red} = \frac{\eta_r - 1}{c} \quad \text{(Equation 6)}$$

The Kraemer Equation (Kraemer 1938) was used to describe the inherent viscosity (η_{inh}) at each concentration:

$$\eta_{inh} = \frac{ln(\eta_r)}{c} \quad \text{(Equation 7)}$$

Lastly, the Solomon-Ciuta Equation (Solomon and Ciută 1962) was used to determine the intrinsic viscosity ([η]), where η_{sp} is the reduced specific viscosity ($\eta_{rel} - 1$):

$$[\eta] \cong \frac{1}{c}(2(\eta_{sp}) - 2\ln(\eta_r))^{1/2} \quad \text{(Equation 8)}$$

Supplementary Material

Refer to Web version on PubMed Central for supplementary material.

Acknowledgements

Funding

Work was performed using National Institutes of Health funding from the National Institute of General Medical Sciences (R01-GM094363) awarded to A.B.H.

References

Brautigam CA (2015) Calculations and publication-quality illustrations for analytical ultracentrifugation data. Methods Enzymol 562:109–133 doi:10.1016/bs.mie.2015.05.001 [PubMed: 26412649]

Brautigam CA, Tso S-C, Deka RK, Liu WZ, Norgard MV (2020) Using modern approaches to sedimentation velocity to detect conformational changes in proteins. European Biophysics Journal 49:729–743 doi:10.1007/s00249-020-01453-w [PubMed: 32761255]

Brookes E, Demeler B, Rosano C, Rocco M (2010) The implementation of SOMO (solution modeller) in the ultrascan analytical ultracentrifugation data analysis suite: Enhanced capabilities allow the reliable hydrodynamic modeling of virtually any kind of biomacromolecule. Eur Biophys J 39:423–435 doi:10.1007/s00249-009-0418-0 [PubMed: 19234696]

Bujacz A (2012) Structures of bovine, equine and leporine serum albumin. Acta Crystallogr D Biol Crystallogr 68:1278–1289 doi:10.1107/s0907444912027047 [PubMed: 22993082]

Byron O (1997) Construction of hydrodynamic bead models from high-resolution x-ray crystallographic or nuclear magnetic resonance data. Biophysical Journal 72:408–415 doi:10.1016/S0006-3495(97)78681-8 [PubMed: 8994627]

Chaton CT, Herr AB (2015) Elucidating complicated assembling systems in biology using size-and-shape analysis of sedimentation velocity data. Methods Enzymol 562:187–204 doi:10.1016/bs.mie.2015.04.004 [PubMed: 26412652]

Chaton CT, Herr AB (2017) Defining the metal specificity of a multifunctional biofilm adhesion protein. Protein Sci 26:1964–1973 doi:10.1002/pro.3232 [PubMed: 28707417]

Comper WD, Preston BN (1992) The analytical ultracentrifuge as a tool for diffusion measurements. Cross diffusion effects in ternary polymer: Polymer: Solvent systems. In: Harding SE, Rowe AJ,

Horton JC (eds) Analytical ultracentrifugation in biochemisty and polymer science. CRC Press, pp 428–442

Conrady DG, Brescia CC, Horii K, Weiss AA, Hassett DJ, Herr AB (2008) A zinc-dependent adhesion module is responsible for intercellular adhesion in staphylococcal biofilms. Proc Natl Acad Sci U S A 105:19456–19461 doi:10.1073/pnas.0807717105 [PubMed: 19047636]

Conrady DG, Wilson JJ, Herr AB (2013) Structural basis for Zn2+-dependent intercellular adhesion in staphylococcal biofilms. Proc Natl Acad Sci U S A 110:E202–211 doi:10.1073/pnas.1208134110 [PubMed: 23277549]

Correia JJ, Lyons DF, Sherwood P, Stafford WF (2016) Techniques for dissecting the johnston-ogston effect. In: Uchiyama S, Arisaka, Stafford WF, Laue T (eds) Analytical ultracentrifugation: Instrumentation, software, and applications. Springer Japan, Tokyo, pp 483–498. doi:10.1007/978-4-431-55985-6_24

Correia JJ, Stafford WF (2015) Chapter three - sedimentation velocity: A classical perspective. In: James LC (ed) Methods in enzymology, vol Volume 562. Academic Press, pp 49–80. doi:10.1016/bs.mie.2015.06.042 [PubMed: 26412647]

Correia JJ, Wright RT, Sherwood PJ, Stafford WF (2020) Analysis of nonideality: Insights from high concentration simulations of sedimentation velocity data. European Biophysics Journal doi:10.1007/s00249-020-01474-5

Creeth JM, Knight CG (1965) On the estimation of the shape of macromolecules from sedimentation and viscosity measurements. Biochimica et Biophysica Acta (BBA) - Biophysics including Photosynthesis 102:549–558 doi:10.1016/0926-6585(65)90145-7

Du Z et al. (2021) The trRosetta server for fast and accurate protein structure prediction. Nat Protoc 16:5634–5651 doi:10.1038/s41596-021-00628-9 [PubMed: 34759384]

Einstein A (1906) Zur theorie der brownschen bewegung. Ann Physik 19:289–305

Einstein A (1911) Bemerkung zu dem gesetz von eötvös. Ann Physik 34:591–593

Elez K, Bonvin AMJJ, Vangone A (2018) Distinguishing crystallographic from biological interfaces in protein complexes: Role of intermolecular contacts and energetics for classification. BMC Bioinformatics 19:438 doi:10.1186/s12859-018-2414-9 [PubMed: 30497368]

Fleming PJ, Correia JJ, Fleming KG (2023) Revisiting macromolecular hydration with HullRadSAS. European Biophysics Journal doi:10.1007/s00249-022-01627-8

Fleming PJ, Fleming KG (2018) HullRad: Fast calculations of folded and disordered protein and nucleic acid hydrodynamic properties. Biophysical Journal 114:856–869 doi:10.1016/j.bpj.2018.01.002 [PubMed: 29490246]

Flodin P (1961) Methodological aspects of gel filtration with special reference to desalting operations. Journal of Chromatography A 5:103–115 doi:10.1016/S0021-9673(01)92827-4

Ghirlando R, Zhao H, Balbo A, Piszczek G, Curth U, Brautigam CA, Schuck P (2014) Measurement of the temperature of the resting rotor in analytical ultracentrifugation. Analytical Biochemistry 458:37–39 doi:10.1016/j.ab.2014.04.029 [PubMed: 24799348]

Harding SE (1995) On the hydrodynamic analysis of macromolecular conformation. Biophysical Chemistry 55:69–93 doi:10.1016/0301-4622(94)00143-8 [PubMed: 17020868]

Harding SE (1997) The intrinsic viscosity of biological macromolecules. Progress in measurement, interpretation and application to structure in dilute solution. Progress in Biophysics and Molecular Biology 68:207–262 doi:10.1016/S0079-6107(97)00027-8 [PubMed: 9652172]

Harding SE, Horton JC, Cölfen H (1997) The ELLIPS suite of macromolecular conformation algorithms. European Biophysics Journal 25:347–359 doi:10.1007/s002490050048 [PubMed: 9213555]

Hayes DB, Stafford WF (2010) Sedview, real-time sedimentation analysis. Macromol Biosci 10:731–735 doi:10.1002/mabi.201000075 [PubMed: 20593366]

Huggins ML (1942) The viscosity of dilute solutions of long-chain molecules. Iv. Dependence on concentration. Journal of the American Chemical Society 64:2716–2718 doi:10.1021/ja01263a056

Jeansonne MS, Foley JP (1991) Review of the exponentially modified gaussian (emg) function since 1983. Journal of chromatographic science 29:258–266 doi:10.1093/chromsci/29.6.258

Juba D, Audus DJ, Mascagni M, Douglas JF, Keyrouz W (2017) Zeno: Software for calculating hydrodynamic, electrical, and shape properties of polymer and particle suspensions. J Res Natl Inst Stand Technol 122:1–2 doi:10.6028/jres.122.020

Jumper J et al. (2021) Highly accurate protein structure prediction with alphafold. Nature 596:583–589 doi:10.1038/s41586-021-03819-2 [PubMed: 34265844]

Kang EH, Mansfield ML, Douglas JF (2004) Numerical path integration technique for the calculation of transport properties of proteins. Phys Rev E Stat Nonlin Soft Matter Phys 69:031918 doi:10.1103/PhysRevE.69.031918 [PubMed: 15089333]

Khasa H, Kilby G, Chen X, Wang C (2021) Analytical band centrifugation for the separation and quantification of empty and full AAV particles. Molecular Therapy - Methods & Clinical Development 21:585–591 doi:10.1016/j.omtm.2021.04.008 [PubMed: 34095342]

Kraemer EO (1938) Molecular weights of celluloses and cellulose derivates. Industrial & Engineering Chemistry 30:1200–1203 doi:10.1021/ie50346a023

Laue TM, Shah BD, Ridgeway TM, Pelletier SL (1992) Computer-aided interpretation of analytical sedimentation data for proteins. In: Harding SE, Rowe AJ, Horton JC (eds) Analytical ultracentrifugation in biochemistry and polymer science. Royal Society of Chemistry, London, pp 90–125

Luo J, Liu Z, Guo Y, Li M (2015) A structural dissection of large protein-protein crystal packing contacts. Sci Rep 5:14214 doi:10.1038/srep14214 [PubMed: 26370141]

Marx DC, Leblanc MJ, Plummer AM, Krueger S, Fleming KG (2020) Domain interactions determine the conformational ensemble of the periplasmic chaperone SurA. Protein Sci doi:10.1002/pro.3924

Monsen RC, Chakravarthy S, Dean WL, Chaires JB, Trent JO (2021) The solution structures of higher-order human telomere g-quadruplex multimers. Nucleic Acids Res 49:1749–1768 doi:10.1093/nar/gkaa1285 [PubMed: 33469644]

Nishihara T, Doty P (1958) The sonic fragmentation of collagen macromolecules. Proc Natl Acad Sci U S A 44:411–417 doi:10.1073/pnas.44.5.411 [PubMed: 16590213]

Philo JS (2000) A method for directly fitting the time derivative of sedimentation velocity data and an alternative algorithm for calculating sedimentation coefficient distribution functions. Anal Biochem 279:151–163 doi:10.1006/abio.2000.4480 [PubMed: 10706784]

Philo JS (2023) Sednterp: A calculation and database utility to aid interpretation of analytical ultracentrifugation and light scattering data. European Biophysics Journal doi:10.1007/s00249-023-01629-0

Plante LD, Romano PM, Fernandez EJ (1994) Viscous fingering in chromatography visualized via magnetic resonance imaging. Chemical Engineering Science 49:2229–2241 doi:10.1016/0009-2509(94)E0046-S

Rocco M, Byron O (2015a) Computing translational diffusion and sedimentation coefficients: An evaluation of experimental data and programs. Eur Biophys J 44:417–431 doi:10.1007/s00249-015-1042-9 [PubMed: 26066679]

Rocco M, Byron O (2015b) Hydrodynamic modeling and its application in AUC. Methods Enzymol 562:81–108 doi:10.1016/bs.mie.2015.04.010 [PubMed: 26412648]

Schneider CM, Cölfen H (2018) Analytical band centrifugation revisited. European Biophysics Journal 47:799–807 doi:10.1007/s00249-018-1315-1 [PubMed: 29931388]

Schneider CM, Haffke D, Cölfen H (2018) Band sedimentation experiment in analytical ultracentrifugation revisited. Analytical Chemistry 90:10659–10663 doi:10.1021/acs.analchem.8b02768 [PubMed: 30160111]

Schuck P (2000) Size-distribution analysis of macromolecules by sedimentation velocity ultracentrifugation and lamm equation modeling. Biophys J 78:1606–1619 doi:10.1016/s0006-3495(00)76713-0 [PubMed: 10692345]

Shelton CL, Conrady DG, Herr AB (2017) Functional consequences of b-repeat sequence variation in the staphylococcal biofilm protein Aap: Deciphering the assembly code. Biochemical Journal 474:427–443 doi:10.1042/bcj20160675 [PubMed: 27872164]

Sherwood PJ, Stafford WF (2016) Sedanal: Model-dependent and model-independent analysis of sedimentation data. In: Uchiyama S, Arisaka F, Stafford WF, Laue T (eds) Analytical

ultracentrifugation: Instrumentation, software, and applications. Springer Japan, Tokyo, pp 81–102. doi:10.1007/978-4-431-55985-6_6

Solomon OF, Ciută IZ (1962) Détermination de la viscosité intrinsèque de solutions de polymères par une simple détermination de la viscosité. Journal of applied polymer science 6:683–686 doi:10.1002/app.1962.070062414

Stafford WF (1992) Boundary analysis in sedimentation transport experiments: A procedure for obtaining sedimentation coefficient distributions using the time derivative of the concentration profile. Analytical Biochemistry 203:295–301 doi:10.1016/0003-2697(92)90316-Y [PubMed: 1416025]

Stafford WF (2016) Analysis of nonideal, interacting, and noninteracting systems by sedimentation velocity analytical ultracentrifugation. In: Uchiyama S, Arisaka F, Stafford WF, Laue T (eds) Analytical ultracentrifugation: Instrumentation, software, and applications. Springer Japan, Tokyo, pp 463–482. doi:10.1007/978-4-431-55985-6_23

Stafford WF, Braswell EH (2004) Sedimentation velocity, multi-speed method for analyzing polydisperse solutions. Biophys Chem 108:273–279 doi:10.1016/j.bpc.2003.10.027 [PubMed: 15043935]

Stafford WF, Sherwood PJ (2004) Analysis of heterologous interacting systems by sedimentation velocity: Curve fitting algorithms for estimation of sedimentation coefficients, equilibrium and kinetic constants. Biophysical Chemistry 108:231–243 doi:10.1016/j.bpc.2003.10.028 [PubMed: 15043932]

Svedberg T, Fåhraeus R (1926) A new method for the determination of the molecular weight of the proteins. Journal of the American Chemical Society 48:430–438 doi:10.1021/ja01413a019

Svedberg T, Lewis NB (1928) The molecular weights of phycoerythrin and of phycocyan. Journal of the American Chemical Society 50:525–536 doi:10.1021/ja01389a042

Svedberg T, Nichols JB (1926) The molecular weight of egg albumin i. In electrolyte-free condition. Journal of the American Chemical Society 48:3081–3092 doi:10.1021/ja01691a008

Svedberg T, Nichols JB (1927) The application of the oil turbine type of ultracentrifuge to the study of the stability region of carbon monoxide-hemoglobin. Journal of the American Chemical Society 49:2920–2934 doi:10.1021/ja01410a046

Vinograd J, Bruner R, Kent R, Weigle J (1963) Band-centrifugation of macromolecules and viruses in self-generating density gradients. Proc Natl Acad Sci U S A 49:902–910 doi:10.1073/pnas.49.6.902 [PubMed: 13997382]

Winzor DJ, Dinu V, Scott DJ, Harding SE (2021) Quantifying the concentration dependence of sedimentation coefficients for globular macromolecules: A continuing age-old problem. Biophys Rev 13:273–288 doi:10.1007/s12551-021-00793-x [PubMed: 33936319]

Wright RT, Hayes D, Sherwood PJ, Stafford WF, Correia JJ (2018) AUC measurements of diffusion coefficients of monoclonal antibodies in the presence of human serum proteins. Eur Biophys J 47:709–722 doi:10.1007/s00249-018-1319-x [PubMed: 30003300]

Yarawsky AE, Herr AB (2020) The staphylococcal biofilm protein Aap forms a tetrameric species as a necessary intermediate before amyloidogenesis. J Biol Chem 295:12840–12850 doi:10.1074/jbc.RA120.013936 [PubMed: 32665400]

Yarawsky AE, Hopkins JB, Chatzimagas L, Hub JS, Herr AB (2022) Solution structural studies of pre-amyloid oligomer states of the biofilm protein Aap. J Mol Biol 434:167708 doi:10.1016/j.jmb.2022.167708 [PubMed: 35777467]

Yarawsky AE, Johns SL, Schuck P, Herr AB (2020) The biofilm adhesion protein Aap from staphylococcus epidermidis forms zinc-dependent amyloid fibers. J Biol Chem doi:10.1074/jbc.RA119.010874

Fig. 1.

Proteins investigated in the current study. Ribbon models are shown for BSA (PDB: 4f5s), Brpt1.5 (PDB: 4fun), and Brpt5.5 (SASBDB: SASPD43). These images were generated using PyMOL (The PyMOL Molecular Graphics System, version 2.4, Schrödinger, LLC).

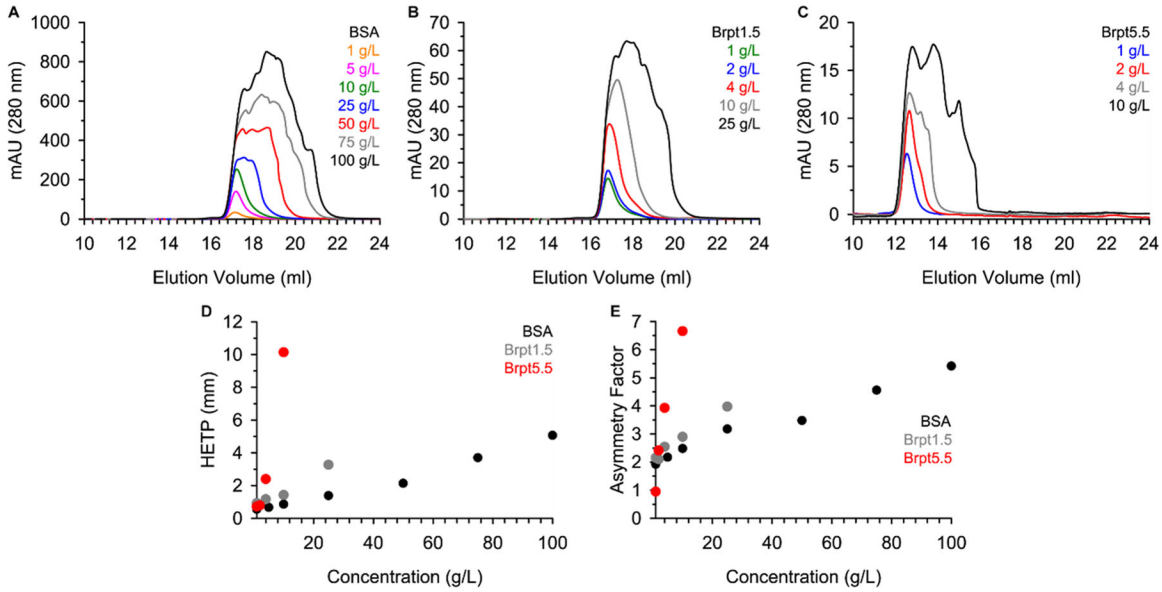

Fig. 2.

Proteins were analyzed by size-exclusion chromatography. SEC chromatograms are shown for (**A**) BSA, (**B**) Brpt1.5, and (**C**) Brpt5.5 at multiple concentrations. The (**D**) HETP and (**E**) asymmetry factor (A_s) were calculated based on each SEC elution profile as described in the Materials and Methods section. Brpt5.5 SEC data (**C**) were previously published (Yarawsky et al. 2022).

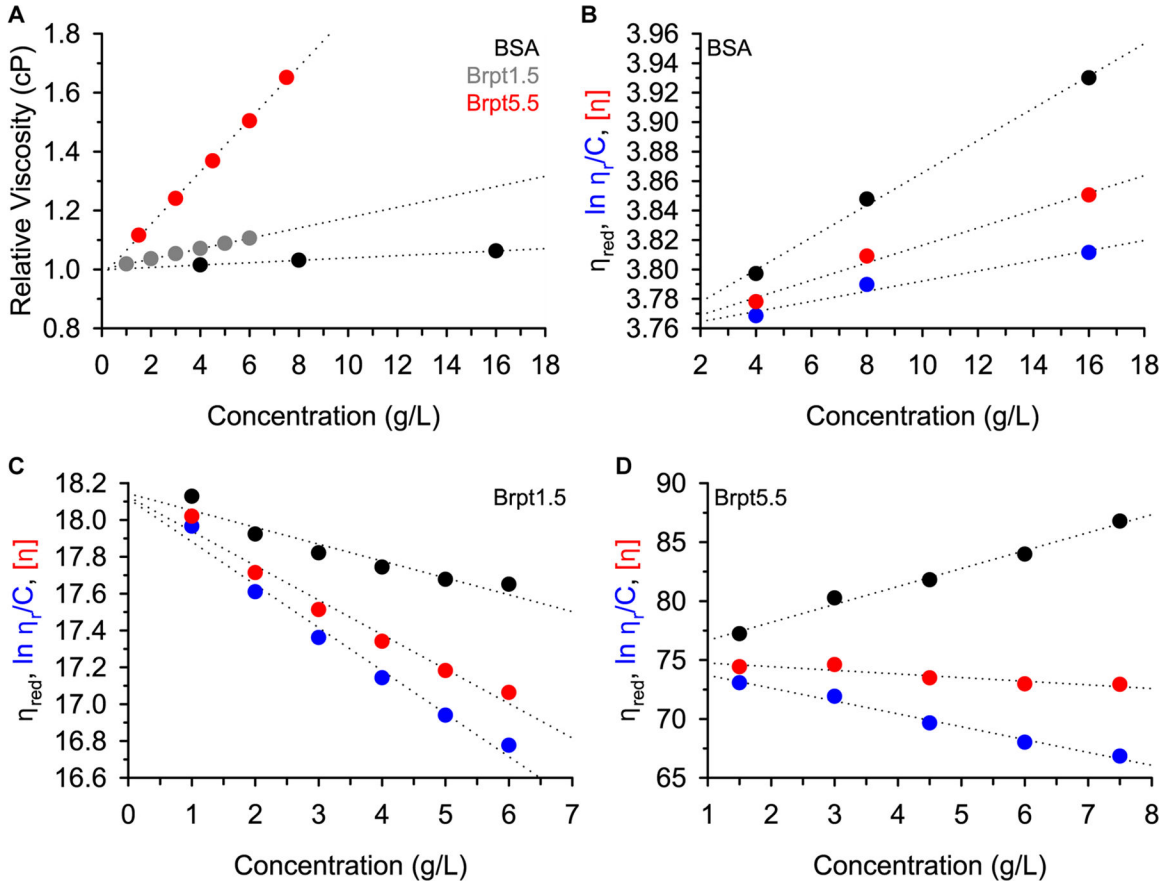

Fig. 3.

Viscosity was measured for each protein at several concentrations. Panel (**A**) shows the relative viscosity data for all three proteins, with markers colored in accordance with the panel legend (BSA = black, Brpt1.5 = grey, Brpt5.5 = red). The reduced viscosity (black), inherent viscosity (blue), and intrinsic viscosity (red) is plotted for BSA in panel (**B**), Brpt1.5 in panel (**C**), and Brpt5.5 in panel (**D**). In all cases, the dotted lines represent linear fits of each dataset.

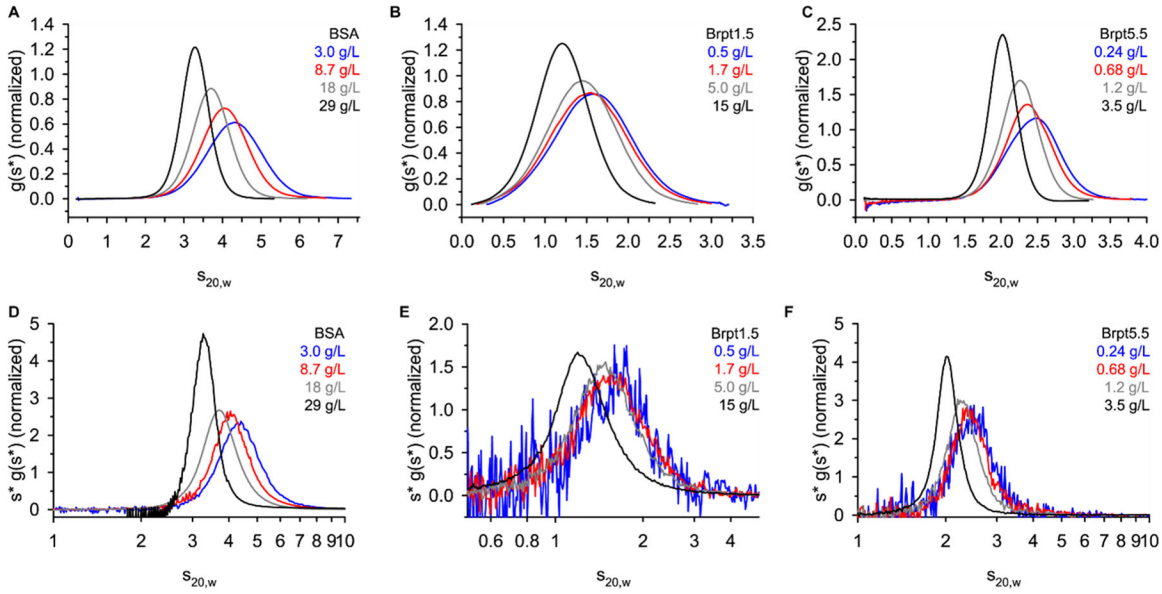

Fig. 4.

Sedimentation velocity AUC data were analyzed by DCDT+ to obtain a g(*s**) distribution (panel **A**-**C**) or by SEDANAL WDA (panel **D**-**F**). Each panel lists the target loading concentration.

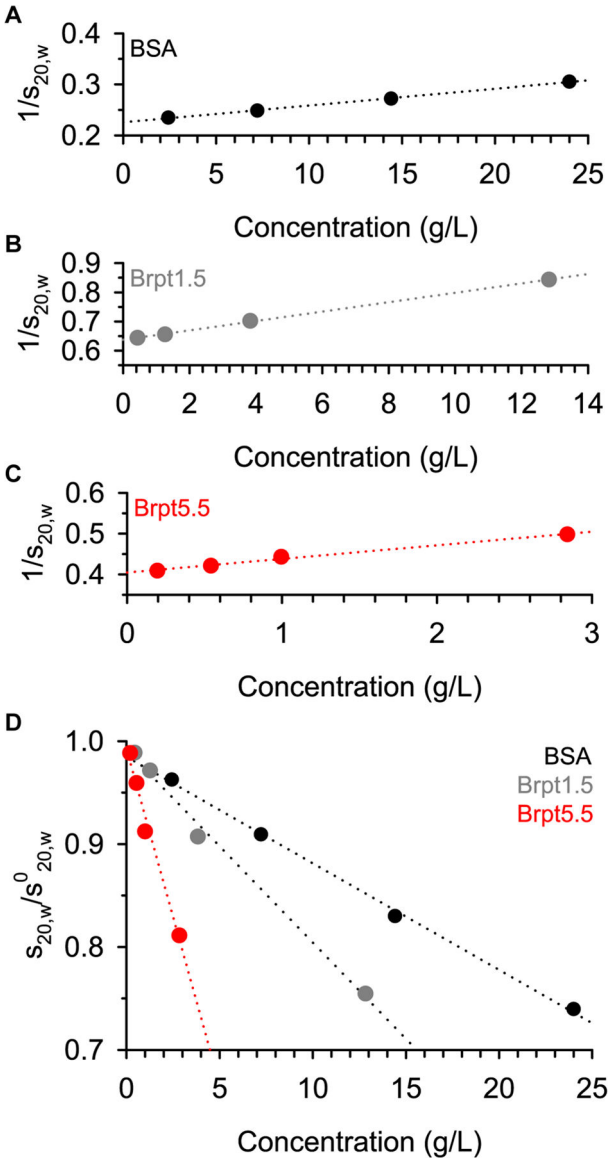

Fig. 5.

Determination of the concentration-dependence of the sedimentation coefficient was performed within SEDNTERP. Sedimentation coefficients used were those reported by integration in DCDT+ after converting to $s_{20,w}$.

Table 1.

Analysis of non-ideal sedimentation

	SEDNTERP		SEDANAL		
	$s^0_{20,w}$	k_s (mL/g)	$s^0_{20,w}$	k_s (mL/g)	BM_1 (mL/g)
BSA	4.43 (4.41 – 4.45)	14.5 (14.1 – 14.9)	4.29 (4.28 – 4.30)	14.7 (14.6 – 14.9)	3.0 (2.5 – 3.5)
Brpt1.5	1.57 (1.57 – 1.58)	25.5 (25.0 – 26.0)	1.54 (1.54 – 1.54)	23.5 (23.5 – 23.6)	12.5 (12.4 – 12.7)
Brpt5.5	2.48 (2.46 – 2.50)	84.0 (77.8 – 90.2)	2.30 (2.30 – 2.31)	68.0 (67.5 – 68.5)	4.4 (0.5 – 8.6)

SEDNTERP error limits are ± 1 standard deviation.

SEDANAL error limits are an estimate of the 95% confidence interval using F-statistics.

Table 2.

Shape parameters determined in the study

	M **(Da)**	$\bar{v}$ **(mL/g)**	**[η]**	***v***	$s^0_{20,w}$	f/f_0
BSA	66,398.00	0.7325	3.8	5.2	4.29	1.3
Brpt1.5	22,217.26	0.7292	18.1	24.8	1.54	1.8
Brpt5.5	78,030.99	0.7280	75.1	103.2	2.30	2.7

	Hydration (g/g)	**P**	***a/b*** **(P)**	**β (x10^6)**	***a/b*** **(β)**	k_s	$k_s/[\eta]$
BSA	0.441	1.1	3.0	1.96	1.0	14.7	3.9
Brpt1.5	0.516	1.5	9.3	2.45	11.7	23.5	1.3
Brpt5.5	0.526	2.3	26.9	2.53	15.1	68.0	0.9

M is the theoretical molar mass based on amino acid composition.

$\bar{v}$ and hydration are based on amino acid composition and reported by SEDNTERP.

For experimental values, *a*/*b* (P) was based on the Perrin function, while *a*/*b* (β) was based on the Scheraga-Mandelkern β function.

$s^0_{20,w}$ and k_S values reported by SEDANAL global fitting to a non-ideal monomer model.

Table 3.

Comparison of experimental results to hydrodynamic modeling

	Experimental						HullRadSAS					AtoB/ZENO			
	$s^0_{20,w}$	f/f_0	a/b (P)	a/b (β)	[η]	k_s	$s^0_{20,w}$	f/f_0	a/b	[η]	k_s	$s^0_{20,w}$	f/f_0	a/b	[η]
BSA	4.29	1.3	3.0	1.0	3.8	14.7	4.42	1.3	1.3	4.5	6.7	4.59	1.3	1.4	3.9
Brpt1.5	1.54	1.8	9.3	11.7	18.1	23.5	1.69	1.7	5.8	18.1	11.5	1.71	1.7	7.0	13.7
Brpt5.5	2.30	2.7	26.9	15.1	75.1	68.0	2.66	2.5	13.7	60.4	31.9	2.47	2.7	15.6	92.1

Models shown in Figure 1 were used for hydrodynamic modeling.

For experimental values, a/b (P) was based on the Perrin function, while a/b (β) was based on the Scheraga-Mandelkern β function.

For AtoB/ZENO calculations, $\overline{v}$ was based on amino acid composition (SEDNTERP).